Associations of increased interstitial fluid with vascular and neurodegenerative abnormalities in a memory clinic sample

Thiel, M.M. van der; Freeze, W.M.; Verheggen, I.C.M.; Wong, S.M.; Jong, J.J.A. de; Postma, A.A.; ... ; Jansen, J.F.A.

Neurobiology of Aging 106 (2021) 257–267

Contents lists available at ScienceDirect

Neurobiology of Aging

journal homepage: www.elsevier.com/locate/neuaging.org

Associations of increased interstitial fluid with vascular and neurodegenerative abnormalities in a memory clinic sample

Merel M. van der Thiel[a,c], Whitney M. Freeze[b,c,d], Inge C.M. Verheggen[b,c], Sau May Wong[a], Joost J.A. de Jong[a,c], Alida A. Postma[a,c], Erik I. Hoff[e], Ed H.B.M. Gronenschild[b,c], Frans R. Verhey[b,c], Heidi I.L. Jacobs[b,f], Inez H.G.B. Ramakers[b,c], Walter H. Backes[a,c,g], Jacobus F.A. Jansen[a,c,h,*]

[a] Department of Radiology & Nuclear Medicine, Maastricht University Medical Center, Maastricht, the Netherlands
[b] Department of Psychiatry &Neuropsychology, Maastricht University, Maastricht, the Netherlands
[c] School for Mental Health & Neuroscience, Alzheimer Center Limburg, Maastricht, the Netherlands
[d] Department of Radiology, Leiden University Medical Center, Leiden, the Netherlands
[e] Department of Neurology, Zuyderland Medical Center Heerlen, Heerlen, the Netherlands
[f] Gordon Center for Medical Imaging, Department of Radiology, Massachusetts General Hospital, Harvard Medical School, Boston, MA, USA
[g] School for Cardiovascular Disease, Maastricht University, Maastricht, the Netherlands
[h] Department of Electrical Engineering, Eindhoven University of Technology, Eindhoven, the Netherlands

ARTICLE INFO

Article history:
Received 28 October 2020
Revised 15 June 2021
Accepted 19 June 2021
Available online 5 July 2021

Keywords:
Alzheimer's disease
Interstitial fluid
Intravoxel incoherent motion
Spectral analysis
Glymphatic system

ABSTRACT

The vascular and neurodegenerative processes related to clinical dementia cause cell loss which induces, amongst others, an increase in interstitial fluid (ISF).

We assessed microvascular, parenchymal integrity, and a proxy of ISF volume alterations with intravoxel incoherent motion imaging in 21 healthy controls and 53 memory clinic patients – mainly affected by neurodegeneration (mild cognitive impairment, Alzheimer's disease dementia), vascular pathology (vascular cognitive impairment), and presumed to be without significant pathology (subjective cognitive decline).

The microstructural components were quantified with spectral analysis using a non-negative least squares method. Linear regression was employed to investigate associations of these components with hippocampal and white matter hyperintensity (WMH) volumes. In the normal appearing white matter, a large f_{int} (a proxy of ISF volume) was associated with a large WMH volume and low hippocampal volume. Likewise, a large f_{int} value was associated with a lower hippocampal volume in the hippocampi.

Large ISF volume (f_{int}) was shown to be a prominent factor associated with both WMHs and neurodegenerative abnormalities in memory clinic patients and is argued to play a potential role in impaired glymphatic functioning.

1. Introduction

The clinical diagnosis of mixed type dementia assumes a spectrum, ranging from cognitive impairment primarily influenced by vascular pathology on one side, to Alzheimer's disease (AD) dementia mainly defined by neurodegeneration on the other side (Emrani et al., 2020). Both vascular and AD-related neurodegenerative processes induce brain tissue damage that is responsible for the development of clinical dementia (van der Flier et al., 2018). These pathologies are associated with underlying processes such as inflammation and edema, which ultimately lead to cell loss, causing amongst others, an increase in interstitial fluid (ISF) (Abbott, 2004; Weller, 1998).

Although many MRI biomarkers have been identified as a proxy specifically for vascular alterations (Rosenberg et al., 2016; Wardlaw et al., 2013) or neurodegeneration (Choi et al., 2019; Dickerson et al., 2009; Moodley and Chan, 2014; Scheltens et al., 1992), few non-invasive MRI measures are sensitive and specific for ISF changes due to cellular alterations.

* Corresponding author at: Department of Radiology & Nuclear Medicine, School for Mental Health and Neuroscience, Maastricht University Medical Center, P.O. box 5800, 6202AZ Maastricht, the Netherlands. Tel.: +31 43 38 74908
E-mail address: jacobus.jansen@mumc.nl (J.F.A. Jansen).

0197-4580/$ – see front matter © 2021 The Author(s). Published by Elsevier Inc. This is an open access article under the CC BY license (http://creativecommons.org/licenses/by/4.0/)
https://doi.org/10.1016/j.neurobiolaging.2021.06.017

Intravoxel incoherent motion (IVIM) provides the opportunity to estimate diffusion components on a microscopic level (Le Bihan et al., 1986). Traditionally, the bi-exponential model is used to quantify two microstructural components from the IVIM signal: the microvascular pseudodiffusion and parenchymal diffusion (Le Bihan et al., 1988; Le Bihan et al., 1986). The microvascular pseudodiffusion (D_{mv}) represents microvascular blood flow within capillaries that approximates a diffusion process, which can subsequently be measured with diffusion imaging. The parenchymal diffusion (D_{par}) represents the motion of water molecules within tissue and generally has a lower speed and amplitude (Le Bihan et al., 1988).

The spectral analysis using the non-negative least squares (NNLS) method lays no constraints on the number of microscopic components that can be estimated by the model and has recently been used to identify a novel, intermediate diffusion component between the two traditional microstructural components (De Luca et al., 2018; Keil et al., 2017; Whittall and MacKay, 1989; Wong et al., 2019). The amplitude of this intermediate component has been previously suggested as a proxy for (increased) ISF volume (Wong et al., 2019). Thereby, IVIM allows for simultaneous investigation of the microvasculature, parenchymal microstructure, and ISF volume.

ISF plays a prominent role in the glymphatic system, a waste-clearance system which has previously been brought in relation to both neurodegeneration and vascular alterations in memory clinic patients (Jessen et al., 2015; Mestre et al., 2017; Rasmussen et al., 2018; Rivera-Rivera et al., 2017). The ability to non-invasively measure ISF volume using spectral analysis, enables further exploration of pathologies associated with glymphatic impairment.

The current study aimed to investigate associations between microscopic diffusion and perfusion components and macroscopic MRI markers of neurodegenerative (i.e., hippocampal atrophy) and vascular (i.e., white matter hyperintensity (WMH) volume) pathology in a memory clinic sample. The applicability of IVIM will be investigated in a memory clinic sample with various degrees of vascular and neurodegenerative pathology. This study simultaneously investigates the microstructure and microvasculature with IVIM in memory clinic patients and healthy controls, covering the whole spectrum of vascular and neurodegenerative pathology, including individuals assumed to be mainly affected by neurodegeneration (mild cognitive impairment, AD dementia), vascular pathology (vascular cognitive impairment) and presumed to be without significant pathology (subjective cognitive decline and healthy controls).

We hypothesize that vascular pathology in terms of white matter hyperintensity volume is associated with increased ISF volume, microvascular changes and decreased parenchymal integrity in the NAWM, a region strongly influenced by vascular processes (Rosenberg, 2009). Furthermore, decreased hippocampal parenchymal integrity and increased ISF volume are foreseen to relate to neurodegeneration in terms of a reduced hippocampal volume (Moodley and Chan, 2014). The intermediate component is thought to be a proxy for ISF increases due to cellular alterations, and therefore is expected to be associated with both macrostructural vascular (WMH volume) and neurodegenerative markers (hippocampal volume) in the NAWM and hippocampi, respectively.

2. Methods

2.2. Participants

To obtain representative variation in WMH volume and hippocampal volume across the spectrum from normal cognition to dementia, cognitively normal older individuals as well as memory clinic patients with various degrees of cognitive impairment were included in this study (Freeze et al., 2019). Neurodegenerative and vascular influences can be viewed as pathological dimensions with arbitrary cut-offs, which in reality show an overlap. Pure vascular dementia (dementia caused solely by vascular pathology) or pure AD dementia (solely caused by AD pathology) are uncommon in clinical practice (Emrani et al., 2020; van der Flier et al., 2018). Therefore, we chose to analyze the memory clinic cohort as a whole, and not separately based on clinical diagnosis.

Patients were recruited at Maastricht University Medical Center and Zuyderland Medical Center. Inclusion criteria for patients were a clinical diagnosis of either subjective cognitive decline (SCD) (Jessen et al., 2014), vascular cognitive impairment (VCI), mild cognitive impairment (MCI) (Petersen, 2004) or clinical AD dementia (McKhann et al., 2011), and mini-mental state examination (MMSE) score $\geq$ 20. Individuals were diagnosed with SCD when self-experienced cognitive decline was reported in comparison with a previously normal status and unrelated to an acute event, but no objective cognitive impairment was detected on any of the neuropsychological tests (Jessen et al., 2014). Individuals were diagnosed with either MCI or VCI – dependent on the expected cause – when concern about cognitive functioning was reported by the patient or an informant, cognitive impairment was detected on at least one cognitive domain, and dementia was absent (Petersen, 2004). Individuals were diagnosed with AD dementia if they met the NIA-AA core clinical criteria for AD dementia (McKhann et al., 2011).

Control participants were recruited through means of advertisement in the local newspaper and online advertisement. Cognitively healthy controls had not visited a memory clinic previously, did not have any cognitive complaints or impairment in memory performance and had a MMSE score $\geq$ 27.

All participants were aged $\geq$ 55 years and did not show any structural abnormalities on MRI, nor had experienced recent (i.e., $<$ 3 months before inclusion) ischemic or haemorrhagic stroke. Further details on inclusion and exclusion criteria are described in Freeze et al. (2019).

2.3. Standard protocol approvals, registrations, and patient consents

Written informed consent was obtained from all participants prior to inclusion. The study protocol was approved by the Medical Ethics Review commission azM / UM (METC) in Maastricht, followed the ethical guidelines of the Dutch Medical Research Involving Human Subjects Act (WMO) and was in line with the Helsinki Declaration of Human Rights. This study was registered at ClinicalTrials.gov (Identifier: NCT02018913; date of registration: December 13, 2013).

2.4. MRI acquisition

All participants underwent a MRI protocol on the same 3.0 Tesla scanner with a 32-channel head coil (Philips, Achieva TX; Philips Healthcare, Best, the Netherlands), as previously described in more detail (Freeze et al., 2019).

Diffusion MR images were acquired using multi-slice single-shot spin-echo echo planar imaging sequence (repetition time (TR) / echo time (TE) = 6800/84 ms; matrix = 112 × 112 × 58; pixel size = 2.4 × 2.4 mm, transverse slice thickness = 2.4 mm) (Wong et al., 2018), with cerebrospinal fluid suppression (inversion time (TI) = 2230 ms). In addition to a non-sensitive b-value of 0 s/mm^2, fourteen diffusion sensitive b-values were employed (b = 5, 7, 10, 15, 20, 30, 40, 50, 60, 100, 200, 400, 700 and 1000 s/mm^2) in three orthogonal directions. Total acquisition time for IVIM imaging was 14 minutes.

A T_1-weighted sequence (TR / TI / TE = 8 / 800 / 4 ms; field of view 256 × 256 × 160 mm^3; 1.0 mm cubic voxel) was performed to image the anatomy of the cerebrum. To visualize WMHs, a T_2-weighted fluid-attenuated inversion recovery sequence (TR / TI / TE = 4800 / 1650 / 290 ms; field of view 250 × 256 × 180 mm^3; 1.0 mm cubic voxel; no slice gap) was used.

2.5. Image processing

Trace images were determined by calculating the average of all three diffusion-sensitive directions and corrected for head displacements, eddy current, and echo planar imaging distortions (ExploreDTI version 4.8.4) (Leemans et al., 2009). Resulting images were smoothed with a Gaussian kernel with a full width at half maximum of 3 mm (FSL version 6.0.1) (Jenkinson et al., 2012).

Anatomical T_1 images were automatically segmented (FreeSurfer version 5.1.0), with visual inspection and manual adjustment when required (Fischl, 2012). WMHs were delineated on the fluid-attenuated inversion recovery images using an in-house developed segmentation tool (Jacobs et al., 2014) and manually checked, as previously described (Freeze et al., 2019). From the segmented images, estimated intracranial volume (ICV), a normal appearing white matter (NAWM) mask, a hippocampi mask (bilateral), and the hippocampal volume (bilateral) were determined. As regions of interest, the hippocampi were chosen considering their prominent influence by neurodegeneration (Fox et al., 1996; Moodley and Chan, 2014), and the total NAWM due to its strong influence by vascular processes (resulting in lesions such as WMHs) (Rosenberg, 2009). Both the hippocampi and NAWM mask were coregistered and spatially down sampled to native IVIM space via the T_1 anatomical images (FLIRT, FSL) (Jenkinson et al., 2002).

2.6. Spectral diffusion analysis

Spectral analysis using NNLS was conducted to analyze the IVIM data in a voxel-based manner, as previously described (De Luca et al., 2018; Keil et al., 2017; Whittall and MacKay, 1989; Wong et al., 2019). Spectral analysis considers the signal to be comprised of a sum of multiple exponentially decaying components that fall within their own range of diffusion components. No constraints are laid on the number of components to be estimated by the model. Based on previous studies (Wong et al., 2019), the spectrum was divided into three ranges: the parenchymal diffusion, $0.1{*}10^{-3} < D < 1.5{*}10^{-3}$ mm^2/s; the intermediate diffusion component (proxy for ISF volume), $1.5{*}10^{-3} \leq D \leq 4.0{*}10^{-3}$ mm^2/s; and the microvascular pseudodiffusion, $4.0{*}10^{-3} < D < 1000{*}10^{-3}$ mm^2/s (Fig. 1). No regularization was applied to the spectrum.

For each voxel, the diffusion values were calculated for the microvascular pseudodiffusion (D_{mv}), the intermediate diffusion (D_{int}) and the parenchymal diffusion (D_{par}) components. D_{mv}, D_{int} and D_{par} were determined by selecting the position of D corresponding to the peaks in the spectrum, and subsequently taking the maxima of the peaks per component. A dictionary of D values was used ranging from $0.1{*}10^{-3}$ to $1000{*}10^{-3}$ mm^2/s with 200 logarithmically spaced values (Wong et al., 2019). The amplitudes per diffusion compartment were defined as the sum of the calculated diffusion values' extension per compartment within the voxel. The least-square based model was constraint to non-negative values, as negative amplitudes have no physiological meaning (Wong et al., 2019). The relative contribution of the intermediate component to the signal (f_{int}) was determined by dividing the amplitude of spectral peaks within the intermediate diffusion range by the sum of the amplitudes of the peaks of the spectrum. The microvascular pseudodiffusion fraction (f_{mv}) was determined in a similar manner, which means that the sum of f_{mv}, f_{int} and the remaining parenchymal diffusion fraction would result in a total of 100% per voxel.

The spectral analysis with NNLS resulted in the following diffusion parameters: the microvascular pseudodiffusion (D_{mv}), which represents the diffusion value of the blood circulating in the microvasculature; the parenchymal diffusion (D_{par}), which represents the diffusion value of the parenchyma; and the intermediate diffusion (D_{int}), which represents the diffusion value of the intermediate component, presumed to be a proxy for ISF. The contribution of the amplitudes falling within each component's range were quantified as a fraction of the sum of all amplitudes in the spectrum. The microvascular pseudodiffusion fraction (f_{mv}) represents the volume fraction of the microvascular signal, and the intermediate component fraction (f_{int}) represents the volume fraction of the ISF component. Only voxels which contained a parenchymal peak were included in the further analysis, and when only an intermediate peak was present, this peak was categorized as falling into the parenchymal range. This correction was applied as it is physiologically unlikely that no parenchyma, but only ISF is present within the ROIs as defined in this study.

f_{mv} and f_{int} were corrected for the inversion pulse and T_1 and T_2 relaxation effects for each quantified component individually (Wong et al., 2019). T_1 and T_2 relaxation properties of the microvascular and parenchymal compartment are retrieved from literature (T_1 = 1624 ms, T_2 = 275 ms and T_1 = 1081 ms, T_2 = 95 ms respectively) (Lu et al., 2004; Simon et al., 2004; Wansapura et al., 1999). The T_1 times of the intermediate component were estimated using an iterative procedure and are voxel-specific, using initialization values of 3000 ms and 1500 ms for T_1 and T_2 values respectively (Wong et al., 2019). To assess whether any clinical group differences in estimated T_1 times of the intermediate component were present, an analysis of variance with Tukey post-hoc analyses was conducted. No significant group differences in estimated T_1 times were identified (Supplementary Table 1). The median values of D_{mv}, f_{mv}, D_{int}, f_{int} and D_{par} were extracted for each parameter within the hippocampi and NAWM.

For comparison purposes, the bi-exponential model was applied to extract the traditional microvascular and parenchymal IVIM parameters (Le Bihan et al., 1988), on which the statistical analyses were applied in a similar manner. The traditional bi-exponential analysis is restricted to the quantification of only two diffusion components (the microvascular pseudodiffusion and parenchymal diffusion), as the combination of only two exponential decay curves are fitted (Le Bihan et al., 1988; Le Bihan et al., 1986).

2.7. Statistical analysis

Multivariable linear regression was employed to investigate the associations of WMH volume and hippocampal volume with the D_{mv}, f_{mv}, D_{int}, f_{int} and D_{par} of the NAWM and hippocampi, while correcting for age, sex and ICV (IBM SPSS statistics version 25). One influential outlier was identified when investigating the association between hippocampal volume and f_{int} in the NAWM (Cook's distance = 2.433) (Supplementary figure 1). However, statistical analyses including and excluding this particular case yielded no substantially different outcomes. Total WMH volume and hippocampal volume were assessed for normality using the Shapiro-Wilk Test. Total WMH volume was calculated per participant and subsequently log-transformed to better approximate a normal distribution. A threshold level of $p < 0.05$ was used to determine sta-

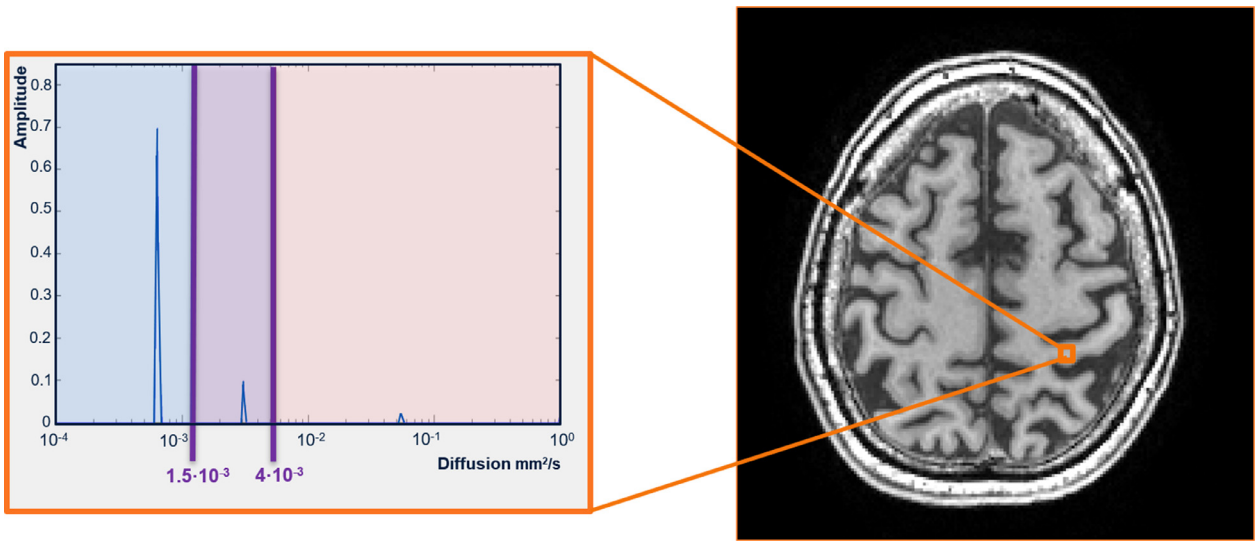

Fig. 1. Example of the diffusion spectrum of a normal appearing white matter voxel in a patient (74 y, female) with Alzheimer's disease dementia. The spectrum is divided into the three diffusion ranges corresponding to signals originating from different brain tissue compartments, with the intermediate diffusion component in the middle. blue = parenchymal diffusion range, purple = intermediate diffusion range, pink = microvascular pseudodiffusion range.

tistical significance. Due to the exploratory nature of the current study, we did not correct for multiple comparisons.

2.8. Data availability

Anonymized data that support the findings of this study are available from the corresponding author, upon reasonable request from any qualified investigator.

3. Results

3.1. Participant characteristics

Seventy-four individuals participated in this study, including patients with AD dementia (n = 15), MCI (n = 16), VCI (n = 9), SCD (n = 13) and healthy controls (n = 21). SCD and control participants were pooled together when displaying demographic characteristics (n = 34). Although the memory clinic cohort was analysed as a whole, sample characteristics including participant- and imaging characteristics and calculated IVIM measures are summarized per clinical group in Table 1.

Figure 2A shows the various degrees of vascular and neurodegenerative pathology present in this cohort, by displaying the variation in WMH volume and hippocampal volume. This figure shows that in general, the control group seems to demonstrate a low WMH volume and high hippocampal volume, while the VCI group predominantly presents with a larger WMH volume and the MCI and AD groups show a lower hippocampal volume. However, no clear clinical cut-offs can be identified as the measures appear to overlap between the different groups, supporting the decision to analyze the memory clinic cohort as a whole, and not separately based on clinical diagnosis. In addition, representative example maps of f_{int} are displayed (Fig. 2B–C), one of a VCI patient with a high WMH load and low hippocampal volume (Fig. 2B) and the other of a control participant with low WMH load and high hippocampal volume (Fig. 2C). The patient with VCI appears to have higher and more extensive f_{int} values in the NAWM (Fig. 2B_1) and hippocampus (Fig. 2B_2) than the control participant (Fig. 2C_1 and C_2 respectively).

3.2. Associations of IVIM measures with WMH and hippocampal volume

3.2.1. Spectral analysis

The associations between WMH and hippocampal volume and the IVIM measures (D_{mv}, f_{mv}, D_{int}, f_{int} and D_{par}) per ROI are provided in Table 2. In the total sample, hippocampal volume was positively associated with D_{int} (β = 0.393, p = 0.001) and negatively associated with f_{int} in NAWM (β = -0.381, p = 0.001). Interestingly, the WMH volume showed the inverse pattern of associations with the same IVIM measures in NAWM (Table 2), where a larger WMH volume related to a higher f_{int} (β = 0.406, $p < 0.001$) and a lower D_{int} (β = -0.270, p = 0.005). Moreover, hippocampal volume and D_{par} of the NAWM showed a negative association. Within the hippocampi, hippocampal volume was negatively associated with f_{int} (β = -0.251, p = 0.032). No other IVIM measures showed any associations with WMH volume or hippocampal volume in any region ($p > 0.05$).

The results did not change after including average absolute displacement as an additional covariate. Similarly, the correction for absolute (aSSR) and relative (rSSR) sum of squared residuals – accuracy measures of NNLS fit – did not alter the results (results not shown). This indicates that the identified associations were not attributable to variation in NNLS fit or subject motion.

3.2.2. The bi-exponential model

When using the traditional bi-exponential model (Le Bihan et al., 1988), similar associations were found concerning the parenchymal diffusion component (Table 3), as were found with the intermediate component using spectral analysis. Using the bi-exponential model, we observed an association of D_{par} in the NAWM with WMH volume (β = 0.296, p = 0.003) and hippocampal volume (β = -0.301, p = 0.014) and in the hippocampi with WMH volume (β = 0.193, p = 0.046) and hippocampal volume (β = -0.517, $p < 0.001$).

Likewise, the same directions of neurodegenerative associations were found in the hippocampi with the microvascular diffusion fraction when using the traditional bi-exponential model (β = -0.267, p = 0.024) (Table 3), as were found in the hippocampi with the intermediate component when using spectral analysis (Table 2).

Table 1
Sample characteristics.

Participant characteristics (n=74)	CON (n=34)	VCI (n=9)	MCI (n=16)	AD (n=15)
Age (years)	69.1 (7.70)	69.7 (5.50)	69.9 (5.01)	70.1 (6.68)
Male, n (%)	18 (52.9)	3 (33.3)	11 (68.8)	10 (66.7)
Education (level)*, median [IQR]	5 [5 – 6]	6 [4 – 6]	5 [4 – 5]	5 [4 – 6]
MMSE score, median [IQR]	29.00 [28.00 – 30.00]	27.00 [25.00 – 29.50]	27.00 [26.25 – 28.00]	26.00 [21.00 – 28.00]+
ApoE4 positive, n (%)	11 (32.4)	6 (66.7)+	7 (43.8)	8 (53.3)
Hypertension, n (%)	16 (47.1)	7 (77.8)	10 (62.5)	8 (53.3)
Diabetes Mellitus, n (%)	1 (2.9)	2 (22.2)	3 (18.8)	2 (13.3)
Cardiovascular disease, n (%)	11 (32.4)	3 (33.3)	5 (31.3)	3 (20.0)
Imaging characteristics				
ICV (cm^3), median [IQR]	1433 [1171 – 1647]	1489 [1380 – 1698]	1539 [1226 – 1629]	1600 [1376 – 1744]
WMH volume (%ICV), median [IQR]	.034 [.022 – .052]	120 [.052 – .212]	.044 [.032 – .080]	.043 [.025 – .068]
HC volume (%ICV), median [IQR]	.040 [.036 – .049]	.035 [.027 – .040]	.030 [.032 – .042]	.029 [.027 – .035]
IVIM measurements				
	Hippocampi / NAWM	Hippocampi / NAWM	Hippocampi / NAWM	Hippocampi / NAWM
Microvascular				
D_{mv} ($x10^{-3}$ mm^2/s)	36 (18) / 51 (14)	35 (14) / 48 (12)	37 (24) / 61 (46)	37 (28) / 59 (17)
f_{mv} (%)	1.6 (.6) / 1.0 (.2)	1.6 (1.0) / 1.0 (.3)	1.9 (1.2) / .9 (.2)	2.0 (.7) / .9 (.2)
Intermediate				
D_{int} ($x10^{-3}$ mm^2/s)	2.6 (.3) / 2.4 (.1)	2.4 (.2) / 2.3 (.1)	2.4 (.3) / 2.3 (.1)	2.6 (.3) / 2.3 (.1)
f_{int} (%)	12.5 (2.1) / 11.0 (1.0)	13.5 (2.9) / 13.1 (2.8)	14.5 (3.1) / 11.7 (1.2)	13.6 (2.4) / 12.0 (1.4)
Parenchymal				
D_{par} ($x10^{-3}$ mm^2/s)	.9 (.1) / .9 (.1)	.9 (.1) / .9 (.1)	.9 (.1) / .9 (.1)	.8 (.1) / .9 (.1)

Mean (standard deviation) is reported unless stated otherwise. Non-zero voxels were excluded to calculate mean diffusion values and the regional means of volume fractions. Subjective cognitive decline participants are classified under the control group. Demographic characteristics are displayed per clinical group solely to display variability within the sample, but further statistical analyses are conducted on the entire sample as a whole.
Abbreviations: CON, Controls; VCI, Vascular cognitive impairment; MCI, Mild cognitive impairment; AD, Alzheimer's disease dementia; ICV, intracranial volume; MMSE, mini-mental state examination; WMH, white matter hyperintensity; NAWM, normal appearing white matter; f_{int}, intermediate peak fraction; D_{int}, intermediate peak diffusion; f_{mv}, microvascular pseudodiffusion fraction; D_{mv}, microvascular pseudodiffusion; D_{par}, parenchymal diffusion.
* Education level was based on an 8-level scale (De Bie and Vegter, 1987).
+ Missing cases = ApoE4 positive, n=1 (VCI); MMSE, n=2 (AD).

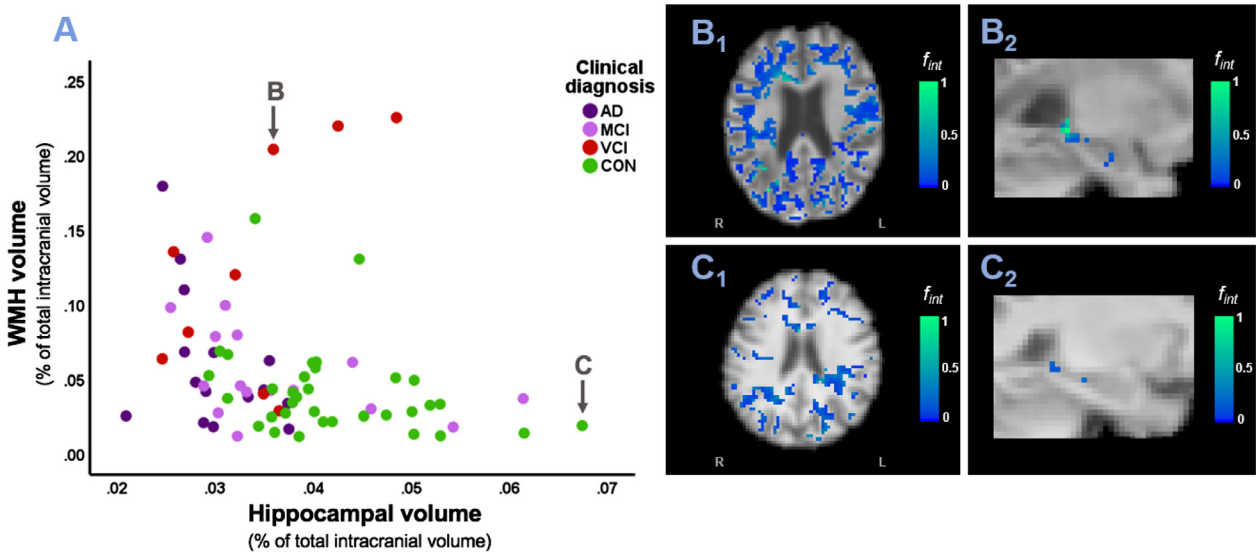

Fig. 2. Scatterplot of white matter hyperintensity and hippocampal volume related to example maps of f_{int}.
A). Scatterplot of WMH volume (% of total intracranial volume – not log-transformed) and hippocampal volume (% of total intracranial volume) values over the patient population, showing the heterogeneity of vascular alterations and neurodegeneration present in the current memory clinic sample. Markers are visualized per clinical group solely to display variability within the sample, but further statistical analyses are conducted on the entire sample as a whole. Subjective cognitive decline participants are classified under the control group. Arrows point to the participants used to present example maps of f_{int}, one being a patient with VCI (*B*) with a high WMH load and low hippocampal volume and the other a control participant (*C*) with low WMH load and high hippocampal volume. **B-C).** Example maps of f_{int} in the NAWM (B_1, C_1) and left hippocampus (B_2, C_2) of a patient with VCI (*B*) and control participant (*C*). The f_{int} maps are overlaid on the T_1w image. Green indicates very high f_{int} values, light blue represents medium to high f_{int} values and dark blue indicates low f_{int} values. Abbreviations: AD, Alzheimer's disease dementia; MCI, mild cognitive impairment; VCI, vascular cognitive impairment; CON, controls; WMH, white matter hyperintensity; NAWM, normal appearing white matter.

Table 2
Associations between vascular and neurodegenerative markers and IVIM measures

	Neurodegenerative marker		Vascular marker	
	Hippocampal volume		WMH volume	
IVIM measures	β	p-value	β	p-value
Hippocampi				
Microvascular				
D_{mv}	0.151	0.202	0.016	0.869
f_{mv}	-0.151	0.203	-0.021	0.831
Intermediate				
D_{int}	0.069	0.569	-0.053	0.597
f_{int}	**-0.251**	**0.032**[a]	0.021	0.836
Parenchymal				
D_{par}	-0.145	0.219	-0.020	0.838
NAWM				
Microvascular				
D_{mv}	-0.135	0.258	0.047	0.640
f_{mv}	0.126	0.313	0.045	0.665
Intermediate				
D_{int}	**0.393**	**0.001**[b]	**-0.270**	**0.005**[a]
f_{int}	**-0.381**	**0.001**[b]	**0.406**	**0.001**[b]
Parenchymal				
D_{par}	**-0.245**	**0.038**[a]	0.113	0.257

WMH volume was log-transformed before the analyses. β represents standardized beta coefficients. Significant associations are depicted in bold and cut-off values are given below. Analyses were adjusted for age, sex and estimated intracranial volume. Abbreviations: D_{int}, intermediate peak diffusion; D_{mv}, microvascular pseudodiffusion; $D_{par,}$ parenchymal diffusion; f_{int}, intermediate peak fraction; f_{mv}, microvascular pseudodiffusion fraction; IVIM, intravoxel incoherent motion; NAWM, normal appearing white matter; WMH, white matter hyperintensity.
[a] $p < 0.05$
[b] $p < 0.01$

Table 3
Associations between vascular and neurodegenerative markers and traditional bi-exponential IVIM measures

	Neurodegenerative marker		Vascular marker	
	Hippocampal volume		WMH volume	
Bi-exponential IVIM measures	β	p-value	β	p-value
Hippocampi				
Microvascular				
D_{mv}	-0.156	0.187	0.044	0.654
f_{mv}	**-0.267**	**0.024**[a]	-0.055	0.580
Parenchymal				
D_{par}	**-0.517**	**<0.001**[b]	**0.193**	**0.046**[a]
NAWM				
Microvascular				
D_{mv}	0.096	0.435	-0.118	0.245
f_{mv}	-0.093	0.469	0.111	0.300
Parenchymal				
D_{par}	**-0.301**	**0.014**[a]	**0.296**	**0.003**[a]

WMH volume was log-transformed before the analyses. β represents standardized beta coefficients. Significant associations are depicted in bold and cut-off values are given below. Analyses were adjusted for age, sex and estimated intracranial volume. Abbreviations: D_{mv}, microvascular pseudodiffusion; $D_{par,}$ parenchymal diffusion; f_{mv}, microvascular pseudodiffusion fraction; IVIM, intravoxel incoherent motion; NAWM, normal appearing white matter; WMH, white matter hyperintensity.
[a] $p < 0.05$
[b] $p < 0.01$

4. Discussion

The current study investigated the relation of microvasculature, interstitial fluid, and parenchymal integrity with vascular (i.e., WMH volume) and neurodegenerative (i.e., hippocampal atrophy) biomarkers in memory clinic patients and controls. By evaluating associations between microscopic tissue alterations and common markers of neurodegenerative as well as vascular pathology (WMH volume) in this mixed study sample, we showed that a large ISF volume is significantly associated with a higher presence of vascular and neurodegenerative biomarkers.

4.1. A large intermediate component volume fraction in NAWM is associated with WMH volume and with hippocampal volume

We found associations of both WMH volume and hippocampal volume with f_{int} in NAWM. A higher amplitude peak within the intermediate component is reflected by a higher f_{int} and is in turn representative of a larger ISF volume in IVIM (Wong et al., 2019). These findings suggest a greater ISF volume to be related to both vascular (WMH volume) and neurodegenerative (hippocampal volume) macroscopic alterations. This study investigated diffusion volume fractions in memory clinic patients, covering a broad spectrum of vascular and neurodegenerative pathology, includ-

ing patients assumed to be principally affected by neurodegeneration (patients with AD and MCI), by vascular pathology (patients with VCI), and presumably without significant pathology (SCD and healthy controls). Although no previous diffusion studies have looked at ISF variations in a memory clinic sample which includes patients who are assumed to be principally affected by AD pathology, Wong et al. (2019) identified a relationship of high f_{int} values with larger WMH volumes in a neurologic outpatient clinic patient sample affected by vascular pathology. In line with their results, our study identified the same positive association between f_{int} values and WMH volume in the NAWM of a memory clinic sample. These findings suggest that f_{int} could be a robust proxy for damage on the cellular level reflecting ISF changes, which in turn is associated with WMH (vascular) pathology. Furthermore, we identified that higher f_{int} values in NAWM was related to hippocampal atrophy, a marker of neurodegenerative alterations.

In addition to the association of higher f_{int} values with larger WMH and smaller hippocampal volume in the NAWM, we observed an association of a lower intermediate diffusion value (D_{int}) in this ROI with both larger WMH and smaller hippocampal volume. When more tissue damage is present, a higher f_{int} will be observed due to the increase in ISF volume related to pathophysiological processes such as neuroinflammation, atrophy and edema (Abbott, 2004; Weller, 1998). Similarly, a lower D_{int} can be observed, as more waste products will be present in the ISF, due to cellular breakdown and the potential presence of toxic proteins (e.g., amyloid beta and tau). Although tissue degradation itself might result in a larger ISF component (a higher f_{int}), the waste products in the extracellular matrix may hinder the diffusion of water molecules, leaving less free space for the water molecules in the ISF to diffuse, subsequently leading to lower intermediate diffusion values. The higher concentration of waste products in the extracellular matrix in damaged regions, will therefore lead to higher f_{int} and lower D_{int} values, regardless of the source of the parenchymal damage (i.e., vascular or neurodegenerative). The strong intrinsic relation between f_{int} and D_{int} might explain the similarity in magnitude of associations found with these parameters, although the associations of f_{int} and D_{int} with the MRI markers were found to be in opposite directions (i.e., negative versus positive). Thereby, this study demonstrated that ISF changes in memory clinic patients are not only related to macroscopic vascular abnormalities (WMH volume) but represent microstructural alterations in the NAWM which are linked to both underlying vascular and neurodegenerative abnormalities.

4.2. Hippocampal atrophy is associated with a large intermediate component volume fraction in the hippocampus

Interestingly, we observed f_{int} in the hippocampi to be associated to the neurodegenerative marker (hippocampal volume), but not to the vascular marker (WMH volume). Consistent with these findings, neurodegenerative influences have been strongly established within this region and the hippocampi are known to be one of the first regions to be affected by atrophy in AD (Fox et al., 1996; Moodley and Chan, 2014). Additionally, our observations are in line with previous results of Maier-Hein et al. (2015), who used the free water (FW) imaging model in patients with MCI and AD dementia to determine a gradual increase in FW (representing the extracellular diffusion contribution) along the progression of AD, which significantly related to atrophy. In the same line of reasoning, there are studies that suggest the hippocampi to be less at risk of vascular alterations (such as WMH) than the NAWM, as a lower presence of WMH is found in the temporal lobe as compared to the other lobes (Gootjes et al., 2004). This difference can be caused by the presence of a more robust vascular network and hippocampal vascular reserve in some patients and the absence of a specific vascular vulnerability of the hippocampi (Gattringer et al., 2012; Perosa et al., 2020). For instance, the study of Perosa et al. (2020) shows that when a mixed vascularization of the hippocampi exists, fewer cSVD markers such as WMH are present. An increased vascular reserve of the hippocampi may be a protective factor for hippocampal structural integrity and cognitive function. While f_{int} in the NAWM seems to be connected to both vascular (WMH volume) and neurodegenerative (hippocampal volume) abnormalities, as expected, hippocampal f_{int} is only associated to neurodegenerative alterations. These findings support f_{int} to be a proxy for damage on the cellular level reflecting ISF changes in the hippocampi, which are in turn associated with hippocampal atrophy and furthermore relate a large ISF volume to local macro-structural alterations.

4.3. WMH volume and hippocampal volume are not associated with the microvascular pseudodiffusion

The current study identified an association of WMH volume and hippocampal volume with f_{int} but found no associations with f_{mv}. The lack of microvascular associations in the current study contrasts with previous memory clinic studies, which did reveal connections between microvascular alterations and AD-related pathology. Multiple arterial spin labeling (ASL) studies have identified a hypoperfusion pattern including both the WM and hippocampi, decreasing along the continuum of AD (Binnewijzend et al., 2016; Hays et al., 2016; Uh et al., 2010; van der Thiel et al., 2019; Zhang et al., 2017). Patients with AD dementia (Binnewijzend et al., 2016; Zhang et al., 2017), patients with MCI (Hays et al., 2016), and even individuals with subtle cognitive decline (van der Thiel et al., 2019) have shown decreased perfusion in previous studies, thereby covering the whole spectrum of memory clinic patients. Although perfusion measures were generally observed to be lower in patients with MCI and AD dementia in WM regions (Uh et al., 2010), hypoperfusion has also been indicated in the hippocampi (Zhang et al., 2017). However, ASL-derived perfusion and IVIM microvascular pseudodiffusion represent different microvascular phenomena (Le Bihan, 2019; Zhang et al., 2018), so caution needs to be taken when comparing our IVIM results with ASL studies. Regardless, these ASL-studies do suggest the occurrence of alterations at a microvascular level in memory clinic patients. ASL-measurements of perfusion might be influenced by variation in the blood supply to the brain (Alsaedi et al., 2018; Okell et al., 2013; van der Thiel et al., 2018), while IVIM's microvascular pseudodiffusion gives a proxy of perfusion independent of variability in blood supply to the brain. Nevertheless, a previous IVIM study also supported the statement of alterations at a microvascular level in memory clinic patients, by demonstrating a decrease in microvascular pseudodiffusion in patients with VCI (Wong et al., 2017).

Several factors can explain the absence of findings that connect vascular (WMH volume) and neurodegenerative (hippocampal volume) markers with the microvascular pseudodiffusion fraction in the hippocampi and NAWM in the current study. For instance, the difference in analysis methods could be responsible for the discrepancy in results concerning the microvasculature from our study and from previous studies. The added value of spectral analysis to analyze microstructural alterations in the brain is discussed in the following section.

4.4. The added value of spectral analysis

Our study implemented spectral analysis using NNLS in a memory clinic sample. Results of previous studies that have used the

bi-exponential model, have indicated a relationship between f_{mv} and vascular and neurodegenerative processes in the hippocampi (van Bussel et al., 2015; Zhang et al., 2019). Similarly, when exploring the bi-exponential model, our memory clinic sample did show an association of hippocampal atrophy with the microvascular component in the hippocampi. Interestingly, when using spectral analysis, the current study did not find an association of hippocampal atrophy with the microvascular component in the hippocampi. Noteworthy, the association of the hippocampal ISF fraction (f_{int}) with hippocampal atrophy found with spectral analysis is shown to be similar as the association of hippocampal atrophy with the hippocampal microvascular pseudodiffusion when the bi-exponential model is used. These findings suggest that when using bi-exponential models, the signal from the intermediate component could be leaking into the nearby microvascular component, biasing IVIM analysis when spectral analysis is not used. This may result in false associations of the microvasculature with macrostructural markers of pathology, which are actually caused by variations in ISF volume.

A previous study by Wong et al. (2017) mentioned enlarged perivascular spaces (PVS) as a potential underlying driver of this biasing effect. When water is flowing in a parallel direction to the vessels, as is the case in PVS, the signal from the PVS can falsely be contributed to the microvascular compartment (Wong et al., 2017). In their study, a larger f_{mv} was found to be associated with enlarged PVS in patients with vascular pathology, further supporting this notion (Wong et al., 2017). Correspondingly, we were unable to find vascular (WMH volume) and neurodegenerative (hippocampal volume) associations with $f_{mv,}$ but did observe vascular and neurodegenerative associations with f_{int} (ISF volume). An increased amount of ISF is argued to be present in enlarged PVS, where ISF can diffuse more freely (Wong et al., 2019). Therefore, the enlargement of the PVS could underlie the observed large f_{int} value (ISF) which is associated with WMH volume and hippocampal volume alterations in the current study.

Similarly, when using a bi-exponential model, associations can be identified of the parenchymal component with WMH and hippocampal volume in both the NAWM and hippocampi, while only an association between the parenchymal component in the NAWM and the hippocampal volume can be observed when the spectral analysis method is used. An impaired parenchyma (D_{par}) estimated using the bi-exponential model, goes hand in hand with larger f_{int} values in the same regions, as observed in the results of the current study using spectral analysis. When the parenchyma disintegrates, the remaining space will likely become more occupied by ISF (Wong et al., 2019). Interestingly, increased extracellular fluid has previously been suggested to be the explanation for observed diffusion alterations which were assumed to indicate loss of parenchymal integrity in memory clinic patients with vascular pathology (Duering et al., 2018). Our findings support this statement, and suggest a larger ISF volume to underly a decreased parenchymal diffusion component (D_{par}) as also observed in memory clinic patients using bi-exponential models. With the current study we were able to simultaneously investigate the parenchymal integrity and ISF volume and subsequently suggest ISF alterations to underlie diffusion alterations that are associated with both WMH volume and hippocampal volume abnormalities.

4.5. The interpretation of the interstitial fluid fraction

Another potential explanation for the observed high f_{int} values associated with WMH volume and hippocampal volume alterations could be the occurrence of microstructural tissue damage, such as neuronal or axonal degeneration and the subsequent loss of the cellular matrix and white matter fibre organization (Maier-Hein et al., 2015). Within our memory clinic sample, microstructural tissue alterations are expected to be the leading factor associated with increased ISF volume, due to prominently observed cell loss within these patient groups (Brun and Englund, 1981; Coleman and Flood, 1987). Therefore, we suggest the loss of tissue microstructure to underlie the observed large f_{int} value, which is associated with WMH and hippocampal volume alterations in the current study.

The observed variations in ISF volume (f_{int}) can be of influence on many mechanisms within the brain, such as the glymphatic system. The glymphatic system is a waste-clearance system which utilizes connecting PVS to efficiently eliminate soluble proteins and metabolites through the brains' ISF (Iliff et al., 2012; Jessen et al., 2015; Mestre et al., 2017; Rasmussen et al., 2018). In line with the results of our study, glymphatic dysfunction has previously been brought in relation to both neurodegeneration and vascular alterations in memory clinic patients (Jessen et al., 2015; Mestre et al., 2017; Rasmussen et al., 2018; Rivera-Rivera et al., 2017). An increase in pulsatility due to reduced vascular compliance has been found in patients with AD dementia, influencing the driving force of the system (Jessen et al., 2015; Rivera-Rivera et al., 2017). Moreover, glymphatic failure renders the brain vulnerable to neurodegeneration and cognitive dysfunction (Jessen et al., 2015). An important consequence of glymphatic dysfunction is that the waste clearance, including amyloid beta removal (Aβ; one of the main pathological hallmarks of AD), is attenuated (Iliff et al., 2012). The potential to measure the ISF volume using spectral analysis with IVIM, opens possibilities to assess glymphatic impairment in memory clinic patients in a non-invasive manner.

4.6. Study considerations

Within our memory clinic sample, the individual diagnostic groups have a limited sample size, particularly the VCI group (n = 9). Due to the clinical and pathological heterogeneity present within the memory clinic sample (Freeze et al., 2019), we chose to examine the study population as a whole using a continuous analytical approach. The mixed underlying pathology present in our study sample is also one of the main strengths of the study. Our sample covered a broad spectrum of vascular and neurodegenerative pathology, including patients assumed to be principally affected by neurodegeneration (patients with AD dementia and MCI), by vascular pathology (patients with VCI), and presumably without significant pathology (SCD and healthy controls), thereby enabling us to investigate both vascular and degenerative associations with microstructural alterations in cognitive decline. However, a limitation of this study is that AD biomarkers amyloid beta and tau were only known for 10 out of 15 patients with AD dementia (66.7%) and the presence of AD pathology was therefore not confirmed with amyloid biomarker evidence for all of them.

Furthermore, the aim of this study was to investigate associations between microscopic diffusion components and neurodegenerative (i.e., hippocampal atrophy) and vascular (i.e., WMH volume) MRI markers in a memory clinic sample. Although - like hippocampal atrophy for neurodegeneration (Fox et al., 1996; Moodley and Chan, 2014; Scheltens et al., 1992) - WMHs are an established MRI marker of vascular pathology (Freeze et al., 2019; Jacobs et al., 2014; Rosenberg, 2009; Wardlaw et al., 2013; Wong et al., 2019), these cannot be labeled as pure vascular markers, due to potential vascular influences leading to neurodegeneration and the interaction of these pathologic processes (Jacobs et al., 2014). In addition, although histopathological studies have long ago indicated microvascular alterations - such as angiofibrosis and arteriosclerosis - to be associated with WMHs, WMHs can also be influenced by other - non-vascular - demyelinating processes such as Wallerian

degeneration or edema (Fazekas et al., 1991; Fazekas et al., 1993). Future studies are necessary to further investigate the complex interplay between neurodegenerative and vascular pathology and validate the specific place of ISF alterations within these pathologic processes.

The spectral analysis approach based on NNLS is a relatively new method and its limitations should also be considered. The ranges of the three components are assumed to be rigid over various brain regions. However, due to the anisotropy of white matter, the diffusivity of parenchymal component strongly varies over regions. For white matter regions with a relatively high fractional anisotropy, the parenchymal diffusivity could be higher than the upper boundary defined for the white matter, thereby leaking into the range defined for the intermediate component. In this study, we have tried to correct for this phenomenon by only including voxels that contain a parenchymal peak. Nonetheless, more research and further algorithm development is needed to account for the regional variability of component ranges.

Within our NNLS approach, a one-to-one relation between the exponential components as estimated with the NNLS and the microscopic compartments is assumed (Wong et al., 2019). Another limitation of our method is that the T_1 and T_2 relaxation properties of the microvascular and parenchymal compartment are retrieved from literature and regionally invariant. However, the T_1 times of the intermediate component are estimated using an iterative procedure and are voxel-specific (Wong et al., 2019). Future studies should further investigate the possibility to obtain quantitative region-specific estimates of T_1 and T_2 to improve correction for relaxation times.

In a previous study of Rydhög et al. (2017), a three-compartment model was used to estimate a parenchymal, microvascular and FW compartment. In their study, the diffusion values per component were predefined based on values derived from the literature. However, as is stated in their discussion, the effective diffusivity of these compartments has been shown to vary in time and space (Federau et al., 2014; Rydhög et al., 2017; Wirestam et al., 2001), and a variety of values are observed in the literature (Federau et al., 2012; Federau et al., 2014; Nicolas et al., 2015; Wirestam et al., 2001). A potential explanation for the variation in diffusion values between studies could also lie in discrepancy in clinical groups, where slower of faster diffusivity might relate to specific disease states. The main advantage of spectral analysis using NNLS in the analysis of IVIM data, is that this approach is data driven. The diffusion values per compartment are determined by the model - within the prespecified diffusion ranges - on which the volume fractions are subsequently calculated. In our study, the diffusion values of ISF/FW (D_{int}) were determined to lie between 2.3–2.6 mm^2/s, However, in the discussed three-compartment model, these were predefined to be 3 mm^2/s, leading to a potential overestimation of this diffusion value when not directly derived from the data. Within the spectral analysis approach, we leave space to estimate the exact diffusion values, which might be beneficial within clinical populations which represent with varying diffusivity within compartments.

In the current study, CSF suppression was applied to suppress the contamination of CSF, while maintaining the ISF signal due to the shorter T_1 time of ISF. Additionally, a potential bias of partial volume effects was minimized by taking the median value per ROI, to ensure that our statistical analysis would not be biased by outlier values. Thereby, we aimed to provide an accurate estimation of the ISF volume per ROI.

Prospective studies in larger patient groups are necessary to explore the potential future usage of the intermediate component as a biomarker for ISF volume associated with different clinical phenotypes of cognitive impairment or distinctive neurological disorders. These studies might be able to investigate the potential of f_{int} as an early biomarker for microscopic damage associated with vascular and neurodegenerative pathology. Moreover, the clinical relevance of f_{int} as a biomarker requires further studies using clinical outcomes.

Furthermore, it is important to note that granting the intermediate component has been previously validated as a potential measure for aberrant amounts of ISF in a patient sample (Wong et al., 2019), the intermediate component as a proxy for ISF volume remains to be verified, for example in animal models, where tissue specimens can be validated microscopically. Although the usage of IVIM imaging seems to have great potential to gain more knowledge on the brains' microstructural composition in a memory clinic sample, prospective histopathological studies are needed to obtain more clarity on the physiological nature of the intermediate diffusion component and to further explore its relationship to glymphatic functioning. As previously suggested by Wong et al. (2019), future studies should investigate the potential of IVIM imaging to detect glymphatic failure by combining IVIM using spectral analysis with measurements of cardiac pulsatility and aquaporin-4 dependent fluid movement.

Furthermore, the current study used three directions for IVIM data acquisition and analyzed the trace image to remove any effects of directionality on the IVIM parameters. However, incorporating direction dependent information of the IVIM diffusion signals might lead to interesting insights in relation to directionality of glymphatic flow patterns.

5. Conclusions

This study validated the applicability of IVIM in a memory clinic sample using spectral IVIM analysis and found associations between microstructural diffusion components and vascular (i.e., WMH volume) and neurodegenerative (i.e., hippocampal volume) MRI markers. We demonstrated that a larger intermediate component (suggested to be a proxy of ISF volume) in NAWM is associated with a larger WMH volume and a lower hippocampal volume. Moreover, we showed a relation between a high hippocampal intermediate component volume fraction and hippocampal atrophy. Thereby, we demonstrated prominent associations of a large intermediate component volume fraction with vascular and neurodegenerative abnormalities and obtained more pathophysiological insights by evaluating microscopic changes in a memory clinic sample influenced by both vascular and AD pathology and by linking them together. Furthermore, our observations might be related to impaired glymphatic functioning associated with the large ISF volume (f_{int}) in memory clinic patients.

Verification

We state that the work described has not been published previously (except in the form of an abstract), that it is not under consideration for publication elsewhere, that its publication is approved by all authors and tacitly or explicitly by the responsible authorities where the work was carried out, and that, if accepted, it will not be published elsewhere in the same form, in English or in any other language, including electronically without the written consent of the copyright-holder.

Disclosure statement

All other authors declare that they have no conflict of interest.

Acknowledgements

M.M. van der Thiel and W.M. Freeze report support from Alzheimer Nederland [grant WE.03-2018-02 and WE.03-2018-13 respectively]. Heidi I.L. Jacobs reports support from Alzheimer Nederland [grant WE.09-2019-02] and the NIH-NIA R01AG06255. A. A. Postma reports support from an institutional grant of Siemens Healthcare and an institutional grant of Bayer Healthcare. The authors disclosed receipt of the following financial support for the research, authorship, and publication of this article: This work was supported by research grants by Alzheimer Nederland [WE.03-2012-40; WE.03-2018-02] and Stichting 2bike4alzheimer.

Supplementary materials

Supplementary material associated with this article can be found, in the online version, at doi:10.1016/j.neurobiolaging.2021.06.017.

CRediT authorship contribution statement

Merel M. van der Thiel: Conceptualization, Methodology, Software, Formal analysis, Visualization, Writing – original draft. **Whitney M. Freeze:** Methodology, Investigation, Writing – review & editing. **Inge C.M. Verheggen:** Investigation, Writing – review & editing. **Sau May Wong:** Software, Writing – review & editing. **Joost J.A. de Jong:** Software, Data curation, Writing – review & editing. **Alida A. Postma:** Investigation, Writing – review & editing. **Erik I. Hoff:** Investigation, Resources, Writing – review & editing. **Ed H.B.M. Gronenschild:** Investigation, Writing – review & editing. **Frans R. Verhey:** Resources, Supervision, Funding acquisition, Writing – review & editing. **Heidi I.L. Jacobs:** Resources, Supervision, Project administration, Funding acquisition, Writing – review & editing. **Inez H.G.B. Ramakers:** Methodology, Supervision, Project administration, Writing – review & editing. **Walter H. Backes:** Methodology, Resources, Supervision, Project administration, Writing – review & editing. **Jacobus F.A. Jansen:** Methodology, Resources, Supervision, Project administration, Funding acquisition, Writing – review & editing.

References

Abbott, N.J., 2004. Evidence for bulk flow of brain interstitial fluid: significance for physiology and pathology. Neurochem Int 45 (4), 545–552.
Alsaedi, A., Thomas, D., Bisdas, S., Golay, X., 2018. Overview and critical appraisal of arterial spin labelling technique in brain perfusion imaging. Contrast Media Mol Imaging 2018, 5360375.
Binnewijzend, M.A., Benedictus, M.R., Kuijer, J.P., van der Flier, W.M., Teunissen, C.E., Prins, N.D., Wattjes, M.P., van Berckel, B.N., Scheltens, P., Barkhof, F., 2016. Cerebral perfusion in the predementia stages of Alzheimer's disease. Eur Radiol 26 (2), 506–514.
Brun, A., Englund, E., 1981. Regional pattern of degeneration in Alzheimer's disease: neuronal loss and histopathological grading. Histopathology 5 (5), 549–564.
Choi, M., Youn, H., Kim, D., Lee, S., Suh, S., Seong, J.-K., Jeong, H.-G., Han, C.E., 2019. Comparison of neurodegenerative types using different brain MRI analysis metrics in older adults with normal cognition, mild cognitive impairment, and Alzheimer's dementia. PloS one 14 (8) e0220739.
Coleman, P.D., Flood, D.G., 1987. Neuron numbers and dendritic extent in normal aging and Alzheimer's disease. Neurobiol Aging 8 (6), 521–545.
De Bie, S.d., Vegter, J., 1987. Standaardvragen 1987 voorstellen voor uniformering van vraagstellingen naar achtergrondkenmerken in interviews. Vereniging van onderzoek instituten (VOI).
De Luca, A., Leemans, A., Bertoldo, A., Arrigoni, F., Froeling, M., 2018. A robust deconvolution method to disentangle multiple water pools in diffusion MRI. NMR Biomed 31 (11), e3965.
Dickerson, B.C., Bakkour, A., Salat, D.H., Feczko, E., Pacheco, J., Greve, D.N., Grodstein, F., Wright, C.I., Blacker, D., Rosas, H.D., 2009. The cortical signature of Alzheimer's disease: regionally specific cortical thinning relates to symptom severity in very mild to mild AD dementia and is detectable in asymptomatic amyloid-positive individuals. Cereb Cortex 19 (3), 497–510.
Duering, M., Finsterwalder, S., Baykara, E., Tuladhar, A.M., Gesierich, B., Konieczny, M.J., Malik, R., Franzmeier, N., Ewers, M., Jouvent, E., Biessels, G.J., Schmidt, R., de Leeuw, F.-E., Pasternak, O., Dichgans, M., 2018. Free water determines diffusion alterations and clinical status in cerebral small vessel disease. Alzheimer's Dementia 14 (6), 764–774.
Emrani, S., Lamar, M., Price, C.C., Wasserman, V., Matusz, E., Au, R., Swenson, R., Nagele, R., Heilman, K.M., Libon, D.J., 2020. Alzheimer's/vascular spectrum dementia: classification in addition to diagnosis. J Alzheimer's Dis 73, 63–71.
Fazekas, F., Kleinert, R., Offenbacher, H., Payer, F., Schmidt, R., Kleinert, G., Radner, H., Lechner, H., 1991. The morphologic correlate of incidental punctate white matter hyperintensities on MR images. Am J Neuroradiol 12 (5), 915–921.
Fazekas, F., Kleinert, R., Offenbacher, H., Schmidt, R., Kleinert, G., Payer, F., Radner, H., Lechner, H., 1993. Pathologic correlates of incidental MRI white matter signal hyperintensities. Neurology 43 (9) 1683-1683.
Federau, C., Maeder, P., O'Brien, K., Browaeys, P., Meuli, R., Hagmann, P., 2012. Quantitative measurement of brain perfusion with intravoxel incoherent motion MR imaging. Radiology 265 (3), 874–881.
Federau, C., O'brien, K., Meuli, R., Hagmann, P., Maeder, P., 2014. Measuring brain perfusion with intravoxel incoherent motion (IVIM): initial clinical experience. J Magn Reson Imaging 39 (3), 624–632.
Fischl, B., 2012. FreeSurfer. Neuroimage 62 (2), 774–781.
Fox, N., Warrington, E., Freeborough, P., Hartikainen, P., Kennedy, A., Stevens, J., Rossor, M.N., 1996. Presymptomatic hippocampal atrophy in Alzheimer's disease: A longitudinal MRI study. Brain 119 (6), 2001–2007.
Freeze, W.M., Jacobs, H.I., de Jong, J.J., Verheggen, I.C., Gronenschild, H., Palm, W.M., Hoff, E.I., Wardlaw, J.M., Jansen, J.F., Verhey, F.R., 2019. White matter hyperintensities mediate the association between blood-brain barrier leakage and information processing speed. Neurobiology of Aging.
Gattringer, T., Enzinger, C., Ropele, S., Gorani, F., Petrovic, K.E., Schmidt, R., Fazekas, F., 2012. Vascular risk factors, white matter hyperintensities and hippocampal volume in normal elderly individuals. Demen Geriatr Cogn Disord 33 (1), 29–34.
Gootjes, L., Teipel, S.J., Zebuhr, Y., Schwarz, R., Leinsinger, G., Scheltens, P., Möller, H.J., Hampel, H., 2004. Regional distribution of white matter hyperintensities in vascular dementia, Alzheimer's disease and healthy aging. Demen Geriatr Cogn Disord 18 (2), 180–188.
Hays, C.C., Zlatar, Z.Z., Wierenga, C.E., 2016. The utility of cerebral blood flow as a biomarker of preclinical Alzheimer's disease. Cell Mol Neurobiol 36 (2), 167–179.
Iliff, J.J., Wang, M., Liao, Y., Plogg, B.A., Peng, W., Gundersen, G.A., Benveniste, H., Vates, G.E., Deane, R., Goldman, S.A., 2012. A paravascular pathway facilitates CSF flow through the brain parenchyma and the clearance of interstitial solutes, including amyloid β. Sci Transl Med 4 (147) 147ra111.
Jacobs, H.I., Clerx, L., Gronenschild, E.H., Aalten, P., Verhey, F.R., 2014. White matter hyperintensities are positively associated with cortical thickness in Alzheimer's disease. J Alzheimer's Dis 39 (2), 409–422.
Jenkinson, M., Bannister, P., Brady, M., Smith, S., 2002. Improved optimization for the robust and accurate linear registration and motion correction of brain images. Neuroimage 17 (2), 825–841.
Jenkinson, M., Beckmann, C.F., Behrens, T.E., Woolrich, M.W., Smith, S.M., 2012. FSL. Neuroimage 62 (2), 782–790.
Jessen, F., Amariglio, R.E., Van Boxtel, M., Breteler, M., Ceccaldi, M., Chételat, G., Dubois, B., Dufouil, C., Ellis, K.A., Van Der Flier, W.M., 2014. A conceptual framework for research on subjective cognitive decline in preclinical Alzheimer's disease. Alzheimer's Demen 10 (6), 844–852.
Jessen, N.A., Munk, A.S.F., Lundgaard, I., Nedergaard, M., 2015. The glymphatic system: a beginner's guide. Neurochem Res 40 (12), 2583–2599.
Keil, V.C., Mädler, B., Gielen, G.H., Pintea, B., Hiththetiya, K., Gaspranova, A.R., Gieseke, J., Simon, M., Schild, H.H., Hadizadeh, D.R., 2017. Intravoxel incoherent motion MRI in the brain: impact of the fitting model on perfusion fraction and lesion differentiability. J Magn Reson Imaging 46 (4), 1187–1199.
Le Bihan, D., 2019. What can we see with IVIM MRI? NeuroImage 187, 56–67.
Le Bihan, D., Breton, E., Lallemand, D., Aubin, M., Vignaud, J., Laval-Jeantet, M., 1988. Separation of diffusion and perfusion in intravoxel incoherent motion MR imaging. Radiology 168 (2), 497–505.
Le Bihan, D., Breton, E., Lallemand, D., Grenier, P., Cabanis, E., Laval-Jeantet, M., 1986. MR imaging of intravoxel incoherent motions: application to diffusion and perfusion in neurologic disorders. Radiology 161 (2), 401–407.
Leemans, A., Jeurissen, B., Sijbers, J., Jones, D., 2009. ExploreDTI: a graphical toolbox for processing, analyzing, and visualizing diffusion MR data. Proc Intl Soc Mag Reson Med 17 (1), 3537.
Lu, H., Clingman, C., Golay, X., Van Zijl, P.C., 2004. Determining the longitudinal relaxation time (T1) of blood at 3.0 Tesla. Magn Reson Med 52 (3), 679–682.
Maier-Hein, K.H., Westin, C.-F., Shenton, M.E., Weiner, M.W., Raj, A., Thomann, P., Kikinis, R., Stieltjes, B., Pasternak, O., 2015. Widespread white matter degeneration preceding the onset of dementia. Alzheimer's Dement 11 (5), 485–493 e482.
McKhann, G.M., Knopman, D.S., Chertkow, H., Hyman, B.T., Jack Jr, C.R., Kawas, C.H., Klunk, W.E., Koroshetz, W.J., Manly, J.J., Mayeux, R., 2011. The diagnosis of dementia due to Alzheimer's disease: recommendations from the National Institute on Aging-Alzheimer's Association workgroups on diagnostic guidelines for Alzheimer's disease. Alzheimer Dement 7 (3), 263–269.
Mestre, H., Kostrikov, S., Mehta, Rupal I., Nedergaard, M., 2017. Perivascular spaces, glymphatic dysfunction, and small vessel disease. Clin Sci 131 (17), 2257–2274.

Moodley, K., Chan, D., 2014. The hippocampus in neurodegenerative disease, The Hippocampus in Clinical Neuroscience. Karger Publishers, pp. 95–108.
Nicolas, R., Sibon, I., Hiba, B., 2015. Accuracies and contrasts of models of the diffusion-weighted-dependent attenuation of the MRI signal at intermediate b-values. Magnetic resonance insights 8, MRI. S25301.
Okell, T.W., Chappell, M.A., Kelly, M.E., Jezzard, P., 2013. Cerebral blood flow quantification using vessel-encoded arterial spin labeling. J Cereb Blood Flow Metab 33 (11), 1716–1724.
Perosa, V., Priester, A., Ziegler, G., Cardenas-Blanco, A., Dobisch, L., Spallazzi, M., Assmann, A., Maass, A., Speck, O., Oltmer, J., 2020. Hippocampal vascular reserve associated with cognitive performance and hippocampal volume. Brain 143 (2), 622–634.
Petersen, R.C., 2004. Mild cognitive impairment as a diagnostic entity. J Intern Med 256 (3), 183–194.
Rasmussen, M.K., Mestre, H., Nedergaard, M., 2018. The glymphatic pathway in neurological disorders. Lancet Neurol 17 (11), 1016–1024.
Rivera-Rivera, L.A., Schubert, T., Turski, P., Johnson, K.M., Berman, S.E., Rowley, H.A., Carlsson, C.M., Johnson, S.C., Wieben, O., 2017. Changes in intracranial venous blood flow and pulsatility in Alzheimer's disease: A 4D flow MRI study. J Cereb Blood Flow Metab 37 (6), 2149–2158.
Rosenberg, G.A., 2009. Inflammation and white matter damage in vascular cognitive impairment. Stroke 40 (3_suppl_1), S20–S23.
Rosenberg, G.A., Wallin, A., Wardlaw, J.M., Markus, H.S., Montaner, J., Wolfson, L., Iadecola, C., Zlokovic, B.V., Joutel, A., Dichgans, M., Duering, M., Schmidt, R., Korczyn, A.D., Grinberg, L.T., Chui, H.C., Hachinski, V., 2016. Consensus statement for diagnosis of subcortical small vessel disease. J Cereb Blood Flow Metab 36 (1), 6–25.
Rydhög, A.S., Szczepankiewicz, F., Wirestam, R., Ahlgren, A., Westin, C.-F., Knutsson, L., Pasternak, O., 2017. Separating blood and water: Perfusion and free water elimination from diffusion MRI in the human brain. NeuroImage 156, 423–434.
Scheltens, P., Leys, D., Barkhof, F., Huglo, D., Weinstein, H., Vermersch, P., Kuiper, M., Steinling, M., Wolters, E.C., Valk, J., 1992. Atrophy of medial temporal lobes on MRI in" probable" Alzheimer's disease and normal ageing: diagnostic value and neuropsychological correlates. J Neurol Neurosurg Psychiatry 55 (10), 967–972.
Simon, J.E., Czechowsky, D.K., Hill, M.D., Harris, A.D., Buchan, A.M., Frayne, R., 2004. Fluid-attenuated inversion recovery preparation: not an improvement over conventional diffusion-weighted imaging at 3T in acute ischemic stroke. Am J Neuroradiol 25 (10), 1653–1658.
Uh, J., Lewis-Amezcua, K., Martin-Cook, K., Cheng, Y., Weiner, M., Diaz-Arrastia, R., Devous, M., Shen, D., Lu, H., 2010. Cerebral blood volume in Alzheimer's disease and correlation with tissue structural integrity. Neurobiol Aging 31 (12), 2038–2046.
van Bussel, F.C., Backes, W.H., Hofman, P.A., van Oostenbrugge, R.J., Kessels, A.G., van Boxtel, M.P., Schram, M.T., Stehouwer, C.D., Wildberger, J.E., Jansen, J.F., 2015. On the interplay of microvasculature, parenchyma, and memory in type 2 diabetes. Diabetes Care 38 (5), 876–882.
van der Flier, W.M., Skoog, I., Schneider, J.A., Pantoni, L., Mok, V., Chen, C.L.H., Scheltens, P., 2018. Vascular cognitive impairment. Nat Rev Dis Primers 4 (1), 18003.
van der Thiel, M., Rodriguez, C., Giannakopoulos, P., Burke, M.X., Lebel, R.M., Gninenko, N., Van De Ville, D., Haller, S., 2018. Brain perfusion measurements using multidelay arterial spin-labeling are systematically biased by the number of delays. Am J Neuroradiol 39 (8), 1432–1438.
van der Thiel, M., Rodriguez, C., Van De Ville, D., Haller, S., Giannakopoulos, P., 2019. Regional cerebral perfusion and cerebrovascular reactivity in elderly controls with subtle cognitive deficits. Front Aging Neurosci 11, 19.
Wansapura, J.P., Holland, S.K., Dunn, R.S., Ball Jr, W.S., 1999. NMR relaxation times in the human brain at 3.0 tesla. J Magn Reson Imaging 9 (4), 531–538.
Wardlaw, J.M., Smith, E.E., Biessels, G.J., Cordonnier, C., Fazekas, F., Frayne, R., Lindley, R.I., O'Brien, J.T., Barkhof, F., Benavente, O.R., Black, S.E., Brayne, C., Breteler, M., Chabriat, H., Decarli, C., de Leeuw, F.-E., Doubal, F., Duering, M., Fox, N.C., Greenberg, S., Hachinski, V., Kilimann, I., Mok, V., Oostenbrugge, R.v., Pantoni, L., Speck, O., Stephan, B.C.M., Teipel, S., Viswanathan, A., Werring, D., Chen, C., Smith, C., van Buchem, M., Norrving, B., Gorelick, P.B., Dichgans, M., nEuroimaging, S.T.f.R.V.c.o., 2013. Neuroimaging standards for research into small vessel disease and its contribution to ageing and neurodegeneration. Lancet Neurol 12 (8), 822–838.
Weller, R.O., 1998. Pathology of cerebrospinal fluid and interstitial fluid of the CNS: significance for Alzheimer disease, prion disorders and multiple sclerosis. J Neuropathol Exp Neurol 57 (10), 885.
Whittall, K.P., MacKay, A.L., 1989. Quantitative interpretation of NMR relaxation data. J Magn Reson 84 (1), 134–152.
Wirestam, R., Borg, M., Brockstedt, S., Lindgren, A., Holtås, S., Ståhlberg, F., 2001. Perfusion-related parameters in intravoxel incoherent motion MR imaging compared with CBV and CBF measured by dynamic susceptibility-contrast MR technique. Acta Radiol 42 (2), 123–128.
Wong, S., Backes, W., Drenthen, G., Zhang, C., Voorter, P., Staals, J., Jansen, J., 2019. Spectral diffusion analysis of intravoxel incoherent motion mri in cerebral small vessel disease. Journal of magnetic resonance imaging. JMRI.
Wong, S., Backes, W., Zhang, C., Staals, J., van Oostenbrugge, R., Jeukens, C., Jansen, J., 2018. On the reproducibility of inversion recovery intravoxel incoherent motion imaging in cerebrovascular disease. Am J Neuroradiol 39 (2), 226–231.
Wong, S.M., Zhang, C.E., van Bussel, F.C., Staals, J., Jeukens, C.R., Hofman, P.A., van Oostenbrugge, R.J., Backes, W.H., Jansen, J.F., 2017. Simultaneous investigation of microvasculature and parenchyma in cerebral small vessel disease using intravoxel incoherent motion imaging. NeuroImage Clin 14, 216–221.
Zhang, C.E., Staals, J., van Oostenbrugge, R.J., Vink, H., 2019. Uncoupling of microvascular blood flow and capillary density in vascular cognitive impairment. Front Neurol 10 1268-1268.
Zhang, N., Gordon, M.L., Goldberg, T.E., 2017. Cerebral blood flow measured by arterial spin labeling MRI at resting state in normal aging and Alzheimer's disease. Neurosci Biobehav Rev 72, 168–175.
Zhang, X., Ingo, C., Teeuwisse, W.M., Chen, Z., van Osch, M.J.P., 2018. Comparison of perfusion signal acquired by arterial spin labeling–prepared intravoxel incoherent motion (IVIM) MRI and conventional IVIM MRI to unravel the origin of the IVIM signal. Magn Reson Med 79 (2), 723–729.